*Advanced Materials Research Vol. 223 (2011) pp 401-410*
*Online available since 2011/Apr/19 at www.scientific.net*

*doi:10.4028/www.scientific.net/AMR.223.401*



# Prediction of Machining Induced Surface Integrity using Elastic-Viscoplastic Simulations and Temperature-Dependent Flow Softening Material Models in Titanium and Nickel-based alloys

D. Ulutan[a], M. Sima[b] and T. Özel[c]
Rutgers University, Manufacturing Automation Research Laboratory,
Department of Industrial and Systems Engineering, Piscataway, New Jersey 08854 USA
[a]dulutan@rutgers.edu, [b]msima@rutgers.edu,[c]ozel@rutgers.edu

**Keywords:** Machining, Surface integrity, Finite Element Method, Titanium alloy, Nickel-Based alloy

## Abstract
In this study, the feasibility of predicting surface integrity and residual stresses by using elasto-viscoplastic finite element simulations and temperature-dependent flow softening constitutive material modeling is investigated. A friction determination method is proposed to identify friction coefficients in presence of tool flank wear. Serrated and cyclical chip formation has been simulated for using tools with and without flank wear. The predicted residual stresses and surface integrity is compared against experimental results from literature. Effect of friction on the residual stress profiles is also investigated. These results are highly essential in predicting machining induced microstructure alterations that are detrimental to fatigue life of nickel and titanium alloy components.

## Introduction
Titanium and nickel alloys are difficult-to-machine materials with considerable manufacturing problems such as machining induce surface integrity and residual stresses [1, 2]. Titanium and its alloys are today used in many industries including aerospace, automotive and medical device. Specifically, Ti-6Al-4V alloy is the most suitable because it offers favorable mechanical characteristics such as high strength-to-weight ratio, toughness, superb corrosion resistance and bio-compatibility. Nickel-base super alloys are often used in mission critical components such as in aircraft/industrial gas turbine engines. Particularly, IN718 nickel alloy is widely utilized and rated as extremely difficult due to the high toughness and work hardening behavior in which a work hardened layer forms in response to the machining induced deformations on the subsurface [3].

When these critical structural components in industry are manufactured with the objective to reach high reliability levels, surface integrity is one of the most relevant parameters used for evaluating the quality of finish machined surfaces. The residual stresses and surface alteration (white etch layer and depth of work hardening) induced by machining of Titanium alloys and Nickel-based alloys are very critical due to safety and sustainability concerns [4]. There are many studies on the issue of surface integrity of machined parts, and an extensive review of such studies has already been done [4-6].

Recently, with the use of modified material behavior models and elasto-viscoplastic deformations based Finite Element (FE) simulations have begun to offer solutions for a rich set of field variables, providing much detailed insight for the chip formation processes in titanium alloys [7,8]. Elasto-viscoplastic FE simulations can also enable realistic prediction of machining induced surface integrity, residual stresses and optimization of tool micro-geometry and machining parameters without running costly experimentation. However, most FE modeling approaches suffer from numerical convergence in elasto-viscoplastic analysis (especially in 3D analysis), lack of reliable material models to represent micromechanical and microstructural changes such as dynamic recrystallization and phase transformation during chip formation and friction characteristics to simulate a realistic chip formation process and accurate calculation of output variables such as strain, stress and temperature distributions. In this paper, elasto-viscoplastic finite element simulations with newly developed material models are utilized to predict machining induced residual stresses on Ti-6Al-4V titanium and IN718 nickel-based alloys.

## Temperature Dependent Flow Softening Material Models

**Titanium Alloy Ti-6Al-4V**. In machining titanium alloys, it is commonly known that plastic instability and adiabatic shearing related chip serration occurs. The underlying cause of chip serration is often associated with adiabatic shearing. Recent studies have considered the effects of flow softening and adiabatic shearing effect on the behavior of titanium Ti-6Al-4V alloy at high strains. Flow softening phenomenon can be described as offering less resistance to local plastic deformations due to rearrangement of dislocations caused by subsequent cycling or dynamic recrystallization in the material. This phenomenon is usually observed during an increase in strain beyond a critical strain value together with a rapid rise in material's temperature. Flow softening is believed to cause adiabatic shearing within the primary shear zone and chip segmentation with shear bands are formed as the deformed material leaves this zone [8]. For this reason, modified material constitutive models with flow softening resulting from strain softening and temperature softening are sought in literature. By developing such a modified Johnson-Cook (JC) constitutive model and implementing it into Finite Element software, Forge-2D by Calamaz et al. [7] and Deform-2D by Sima and Özel [8] were able to simulate serrated chip formation in machining of titanium alloy Ti-6Al-4V. In the modified JC material model given in Eq. (1), the influence of strain, strain rate, temperature and temperature dependent strain softening on the flow stress is defined by four multiplicative terms.

$$\sigma = \left[A + B\varepsilon^{n}\left(\frac{1}{\exp(\varepsilon^{a})}\right)\right]\left[1 + C\ln\frac{\dot{\varepsilon}}{\dot{\varepsilon}_0}\right]\left[1 - \left(\frac{T-T_0}{T_m-T_0}\right)^{m}\right]\left[D + (1-D)\left[\tanh\left(\frac{1}{(\varepsilon+p)^{r}}\right)\right]^{s}\right] \qquad (1)$$

where $D = 1 - \left(\frac{T}{T_m}\right)^{d}$, $p = \left(\frac{T}{T_m}\right)^{b}$, $\sigma$ is flow stress, $\varepsilon$ is true strain, $\dot{\varepsilon}$ is true strain rate, $\varepsilon_0$ is reference true strain, and T, $T_m$, $T_0$ are work, material melting and ambient temperatures respectively. The experimental flow stress data by Lee and Lin [9] has been taken as the base for this modified material model. The most optimum set of model parameters that was identified with inverse analysis are; A=724.7 MPa, B=683.1 MPa, n=0.47, C=0.035, m=1.0, Tm=1604°C, a=2, s=0.05, r=2, d=1, b=5. The details of this methodology are outlined by Sima and Özel [8] and flow stress curves are given in Fig.1.

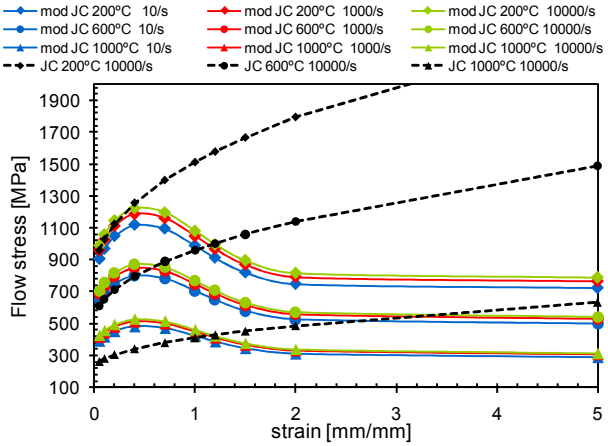


Fig. 1: Modified flow stress curves for Ti-6Al-4V versus the JC model by Lee and Lin [9].

**Nickel Based Alloy IN718**. On the other hand, dynamic material behavior data for Inconel 718 do not appear in the published literature with a very few exceptions. Zhang et al. [10] investigated strain-rate sensitivity of IN718 at high temperatures and presented compression test results at temperatures from 960 to 1040°C, with strain rates from 0.001 to 1.0 $s^{-1}$. One of the revealing results of that study was the flow softening behavior of the flow stress curve at strain rate of 1.0 $s^{-1}$ and temperature of 980°C above the strain value of 0.3. DeMange et al. [11] have studied high strain rate compression behavior of IN718 under annealed and aged conditions at strain rate ranges of 1796-3506 $s^{-1}$ for annealed and 1681-4581 $s^{-1}$ for aged IN718 material. Flow stress curves of the annealed material exhibited strong strain hardening at all strains, but the curves of the aged material showed sharp softening effect around a strain value of 0.1 and remained constant after strain value of 0.25. Pereiera and Lerch [12] referred to that data and suggested the JC constitutive model without considering thermal softening effects (A= 1350 MPa, B= 1139 MPa, n= 0.6522, C= 0.0134) for

aged IN718 material. Uhlmann et al. [13] also utilized the Johnson-Cook material model to simulate cutting of annealed IN718 and used model parameters proposed by Sievert et al. [14] and Olschewski et al. [15]. These parameters (A=450 MPa, B=1700 MPa, C=0.017, n=0.65, m=1.3) for annealed IN718 material included a thermal softening exponent as well. However Lorentzon et al. [16] used the JC model parameters A, B, C, n from Mitrofanov et al. [17] and m=1.3 from [14] and [15] for aged IN718 material. Modified JC material model is considered to represent temperature dependent flow softening behavior of IN718 nickel based alloy since flow softening phenomenon is also reported for it [10-12]. Hence, modified material model given in Eq. (1) was employed for IN718 material to include the temperature-dependent flow softening effect in addition to strain and strain rate hardening and thermal softening. The model parameters for IN718 are identified as A= 1350 MPa, B= 650 MPa, n= 0.6522, C= 0.0134, m = 1.3, a=4, d=0.1, b=2, r=1, s=0.01 and melting temperature is taken as $T_m$=1297 $^0$C. The flow stress curves are given in Fig.2.

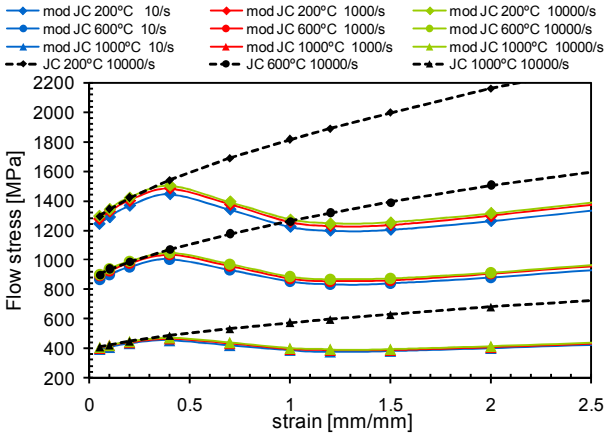


Fig. 2: Modified flow stress curves for IN718 versus the JC model by Lorentzon et al. [16].

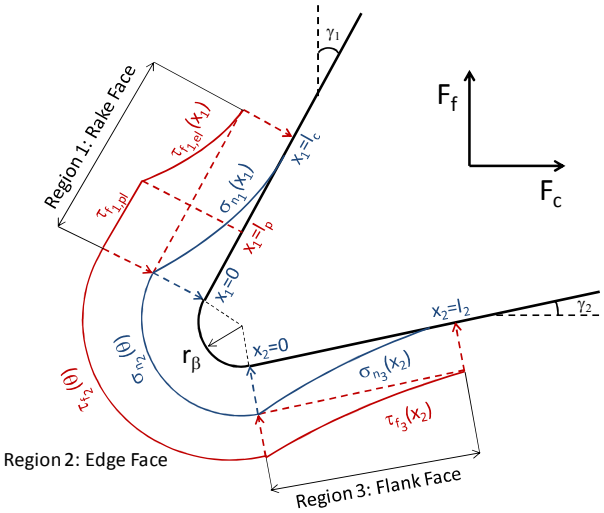


Fig. 3: Illustration of stress distributions along the round edge tool faces.

## A Friction Determination Model for Round Edge Cutting Tools

A friction model for the round edge tool is developed. The goal is to obtain a universal friction model so that the rake and flank face friction coefficients can be determined in the presence of tool flank wear. For this purpose, the tool-workpiece/chip interface was divided into three regions (see Fig. 3). Tool and workpiece were considered to have full contact on the edge face, where the workpiece faces shearing. In this region, slip conditions of friction are assumed. From the rake end of the circular region ($x_1$=0) to the end of the tool/chip contact ($x_1$=$l_c$), tool and workpiece were considered to have slip and slide friction conditions. From the flank end of the circular region ($x_2$=0) to the end of the wear length ($x_2$=$l_2$), the tool is assumed to have only sliding friction conditions. The sliding friction coefficients at the rake and flank faces are calculated using the procedure described below, in order to be employed in FE modeling. When there is no flank wear (fresh/new tool), it is assumed

that the tool only has two regions of applied normal and shear stress, rake and edge faces. The forces on these regions are calculated as described below, and the components in cutting and feed directions are summed up in order to calculate the total force in both directions.
To start the procedure, five unknown variables are searched within acceptable intervals: rake and flank face friction ($\mu_1$ and $\mu_2$, respectively), tool-chip contact length on the rake region ($l_c$), maximum normal stress on the rake region ($\sigma_{n1,max}$), and the maximum normal stress on the flank region ($\sigma_{n3,max}$). The normal and tangential components of forces in all three regions are calculated and converted to cutting ($F_c$) and feed ($F_f$) force components, which are then summed up to result in the total cutting and feed forces:

$$F_c = F_{n1,c} + F_{t1,c} + F_{n2,c} + F_{t2,c} + F_{n3,c} + F_{t3,c} \quad (2)$$

$$F_f = F_{n1,f} + F_{t1,f} + F_{n2,f} + F_{t2,f} + F_{n3,f} + F_{t3,f} \quad (3)$$

Here, in the first region, normal stress is assumed to have a polynomial distribution:

$$\sigma_{n1} = \sigma_{n1,max}\left(1 - \frac{x_1}{l_c}\right)^n \quad (4)$$

When integrated from $x_1$=0 to $x_1$=$l_c$, the normal component of the force in this region is found to be:

$$F_{n1} = \sigma_{n1,max}\frac{l_c}{n+1} \quad (5)$$

There are two different types of friction in this region. The sticking friction brings plastic shear conditions, which equals to $\tau_{f1,pl}$. After a certain amount of plastic contact, the chip starts to slide on the tool, which brings elastic shear conditions. Here, the shear stress is related to the normal stress by the equation:

$$\tau_{f1,el}(x_1) = \mu_1\sigma_{n1}(x_1) \quad (6)$$

So, the plastic shear stress can be found as:

$$\tau_{f1,pl} = \mu_1\sigma_{n1,max}\left(1 - \frac{l_p}{l_c}\right)^n \quad (7)$$

Then, after integrating the shear stresses from $x_1$=0 to $x_1$=$l_c$, the total tangential force in this region can be found as:

$$F_{t1} = \mu_1\sigma_{n1,max}l_p\left(1 - \frac{l_p}{l_c}\right)^n + \mu_1\sigma_{n1,max}\left(\frac{l_c}{n+1}\right)\left(1 - \frac{l_p}{l_c}\right)^{n+1} \quad (8)$$

In the second region, the normal and shear stresses are assumed to be linearly changing throughout the angular profile (Fig. 4). The normal stresses start from $\sigma_{n1,max}$ at $\theta$=-$\gamma_1$, and decrease linearly to $\sigma_{n3,max}$ at $\theta$=$\pi$/2+$\gamma_2$ (Fig. 5). If the tool is unworn, $\sigma_{n3,max}$ is assumed to be zero. Hence, the normal stress distribution in the second region can be written as:

$$\sigma_{n2} = \frac{(\sigma_{n3,max} - \sigma_{n1,max})\theta}{\frac{\pi}{2}+\gamma_1+\gamma_2} + \frac{\gamma_1\sigma_{n3,max} + \left(\frac{\pi}{2}+\gamma_2\right)\sigma_{n1,max}}{\frac{\pi}{2}+\gamma_1+\gamma_2} \quad (9)$$

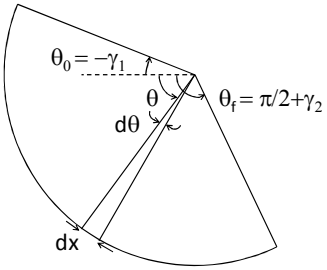


Fig. 4: Edge face illustration.

The shear stress, on the other hand, starts from $\tau_{f1,pl}$ at $\theta$=-$\gamma_1$, and decrease linearly to $\tau_{f3,max}$ at $\theta$=$\pi$/2+$\gamma_2$ (Fig. 6).

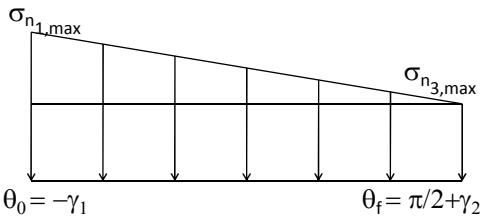

Fig. 5: Normal stresses on the face of the round edge.

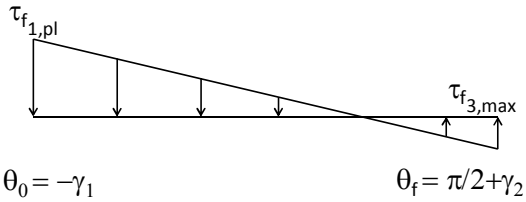

Fig. 6: Shear stresses on the face of the round edge.

The shear stress at $\theta=\pi/2+\gamma_2$ is assumed to be zero, when the tool is unworn. If the tool is worn, this stress is assumed to be at the opposite direction of rake face shear stress, causing a stagnation point at the edge face. When the tool is unworn, the stagnation point is assumed to be at $\theta=\pi/2+\gamma_2$. Therefore, the shear stress distribution in the second region can be written as:

$$\tau_{f2} = -\frac{(\tau_{f3,max}+\tau_{f1,pl})\theta}{\frac{\pi}{2}+\gamma_1+\gamma_2} - \frac{\gamma_1\tau_{f3,max}-\left(\frac{\pi}{2}+\gamma_2\right)\tau_{f1,pl}}{\frac{\pi}{2}+\gamma_1+\gamma_2} \quad (10)$$

From these normal and shear stresses, the components of forces in the second region in cutting and feed directions can be found. The forces in the third region can be found similarly to the first region, except here, there is no sticking condition assumed. After all the forces are calculated, they are summed up in cutting and feed directions, and compared to the test data of Wyen and Wegener [18]. The searched variables are optimized according to the measured data, and according to this search, the friction coefficient values that resulted in the minimum difference between the measured and calculated forces were accepted as the Coulomb friction coefficients in corresponding regions. After comparing the results with the measurements of Wyen and Wegener [18], the normalized non-linear relationships between the two friction coefficients (rake face, $\mu_1$ and flank face $\mu_2$) and cutting velocity ($v_c$), feed rate ($t_u$), and cutting edge radius ($r_\beta$) were found to be:

$$\mu_i = a_i(v_c) + b_i(t_u) + c_i(r_\beta) + d_i(v_c t_u) + e_i(v_c r_\beta) + f_i(t_u r_\beta) + g_i(v_c t_u r_\beta) + h_i \quad (11)$$

where the coefficients are given in Table 1.

| | a | b | c | d | e | f | g | h |
|---|---|---|---|---|---|---|---|---|
| $\mu_1$ | -0.08 | -0.12 | 0.5 | 0.01 | 0.02 | -0.03 | 0.01 | 0.66 |
| $\mu_2$ | 0.04 | 0.12 | -0.17 | -0.03 | -0.03 | 0.08 | -0.02 | 1 |

Table 1: Coefficients of the non-linear relationships for rake and flank face friction coefficients

As also depicted by the coefficients of the equations, it was found that rake face friction coefficient ($\mu_1$) decreases when the feed rate is increased, increases significantly when the cutting edge radius is increased, and decreases slightly when the cutting speed is increased, with the non-linear terms being insignificant compared to the linear terms. On the other hand, the flank face friction coefficient ($\mu_2$) increases slightly with increasing feed rate, does not change significantly with the cutting speed, and decreases significantly with increasing cutting edge radius at lower feed rates (0.06 mm) but decreases only slightly with increasing cutting edge radius at higher feed rates (0.2 mm). This is reflected on the non-linear term that includes the feed rate and the cutting edge radius ($f_2$) being considerably higher than the other coefficients when normalized. This formula (Eq. (11)) can be assumed to represent the interval where $v_c$ =10-110 m/min, $t_u$=0.06-0.2 mm, $r_\beta$=10-50 μm, since the measured data used covers this interval. This formula can then be utilized to find the coefficients of

friction at the rake and flank faces at $v_c$ =55 m/min and $v_c$= 90 m/min, $t_u$=0.15 mm, $r_\beta$=30 μm. These coefficients of friction are inserted into the calculations of cutting forces to estimate the applied forces during machining, as well as the stresses, strains, and temperature field on the tool, leading to other significant results. When the values are calculated, forces in the cutting and feed directions are found as shown in Table 2, as well as the friction coefficients in both rake and flank faces. Therefore, the friction coefficients solved for Ti-6Al-4V alloy are utilized in FE simulations.

Table 2: Coefficients of friction and forces at $t_u$=0.15 mm and $r_\beta$=30μm.

| $v_c$ [m/min] | $\mu_1$ | $\mu_2$ | $\sigma_{1,max}$ [MPa] | $\sigma_{3,max}$ [MPa] | $F_c$ [N] | $F_f$ [N] |
|---|---|---|---|---|---|---|
| 55 no flank | 0.6011 | 0 | 974 | 0 | 657 | 349 |
| 90 no flank | 0.5904 | 0 | 988 | 0 | 667 | 349 |
| 55 flank | 0.6011 | 0.505 | 974 | 6.08 | 727 | 502 |
| 90 flank | 0.5904 | 0.4882 | 988 | 592 | 747 | 526 |

**Finite Element Modeling**

In this study, finite element (FE) simulations are also developed using updated Lagrangian software (DEFORM-2D) in which chip separation from workpiece is achieved with continuous remeshing. Throughout this study, only coupled *thermo elasto-viscoplastic* finite element simulations are considered. These elasto-viscoplastic simulations included a workpiece as elasto-viscoplastic with a mesh containing 10000 quadrilateral elements with element size ranging from 2 μm to 60 μm. Uncoated carbide (WC/Co) tool is modeled as rigid with a mesh containing into 2500 elements. A high density mesh in the primary deformation zone was applied. A rake angle of $\gamma_1$=6°, a flank/clearance angle of $\gamma_2$=7°, and edge radius of $r_\beta$=30 μm for tool are employed in the tool geometry. Thermal boundary conditions are defined accordingly in order to allow heat transfer from workpiece to the cutting tool. The heat conduction coefficient ($h$) is taken as $10^5$ $kWm^{-2}K^{-1}$ to allow rapid temperature rise in the tool. Mechanical and thermo-physical properties of titanium Ti-6Al-4V alloy and IN718 nickel alloy are defined as temperature-dependent ($T$ in ºC). Temperature -dependent modulus of elasticity ($E$ in MPa), thermal expansion (α in $mm.mm^{-1}.°C^{-1}$), thermal conductivity (λ in $W.m^{-1}.°C^{-1}$), and heat capacity ($c_p$ in $N.mm^{-2}.°C^{-1}$) are given in Table 3.

As explained in the friction determination model, friction around the tool faces is sophisticated when round edge inserts are employed. At the rake face, friction factor decreases with increasing ratio of uncut chip thickness ($t_u$) to edge radius ($r_\beta$) and increasing cutting speed ($v_c$). Similarly in the FE model, three contact regions around the round edge of the tool with the workpiece are considered: (i) a sticking contact around the round edge curvature ($\tau_f$=$k$ or $m$=$\tau_f/k$=1 where $k$ is the work material shear flow stress), (ii) along the rake face; a shear friction contact ($m$=0.9) and a sliding friction contact ($\mu_1$) along the rest of the tool-chip interface, and (iii) a sliding friction contact along the flank face ($\mu_2$). Along rake face, shear friction and sliding friction regions are employed by using the hybrid friction capability in DEFORM-2D software. The cutting conditions and the friction coefficients employed in FE simulations are given in Table 4. The results of the FE simulations are summarized in Table 5. Average cutting ($F_c$) and feed/thrust ($F_f$) forces are predicted in a range (e.g. $F_{c\text{-}valley}$ - $F_{c\text{-}peak}$) and average chip thickness ($t_{c\text{-}ave}$) along with chip compression ratios (CCR) are given. Maximum work temperature ($T_w$) is also given. The influence of flank face friction coefficient in the presence of flank wear is also shown. The effects of flank wear on predicted chip formation and temperatures are given in Fig. 7.

Table 3: Properties of work and tool materials.

| | Ti-6Al-4V | IN718 | WC/Co |
|---|---|---|---|
| E($T$) | $0.7412*T+113375$ | $-61000*T+278000$ | $5.6*10^5$ |
| α($T$) | $3.10^{-9}*T+7.10^{-6}$ | $10^{-5}*e^{0.0849*T}$ | $4.7*10^{-6}$ |
| λ($T$) | $7.039*e^{0.0011*T}$ | $10.409*e^{0.0903*T}$ | 55 |
| $c_p$($T$) | $2.24*e^{0.0007*T}$ | $418.63*e^{0.0433*T}$ | $0.0005*T+2.07$ |

Table 4: Cutting conditions and friction used.

| | Ti-6Al-4V titanium alloy | | IN718 nickel-based alloy | |
|---|---|---|---|---|
| $v_c$[m/min] | 55 | 90 | 55 | 90 |
| $t_u$ [mm] | 0.15 | 0.15 | 0.15 | 0.15 |
| VB [mm] | 0.14 | 0.14 | 0.24 | 0.24 |
| $\mu_1$ | 0.6 | 0.6 | 0.6 | 0.6 |
| $\mu_2$ | 0.4, 0.5, 0.6 | 0.4, 0.5, 0.6 | 0.4, 0.5, 0.6 | 0.4, 0.5, 0.6 |

Table 5: Summary of the FE simulation results

| Simulation | | *ave.* $F_c$ (range) | *ave.* $F_f$ (range) | $t_{c\text{-}ave}$ [mm] | *CCR* | $T_w$[°C] |
|---|---|---|---|---|---|---|
| Ti64-55 m/min | *unworn* | 264(230-298) | 127(114-140) | 0.185 | 0.144 | 651 |
| | $\mu_2$=0.4 | 244(214-275) | 109( 99-119) | 0.160 | 0.163 | 639 |
| | $\mu_2$=0.5 | 249(218-280) | 109(100-118) | 0.159 | 0.157 | 632 |
| | $\mu_2$=0.6 | 251(222-281) | 111(102-120) | 0.160 | 0.156 | 641 |
| Ti64-90 m/min | *unworn* | 256(219-292) | 117(103-130) | 0.184 | 0.166 | 721 |
| | $\mu_2$=0.4 | 251(219-282) | 114(103-125) | 0.162 | 0.198 | 682 |
| | $\mu_2$=0.5 | 242(211-273) | 104( 97-112) | 0.157 | 0.172 | 724 |
| | $\mu_2$=0.6 | 247(218-276) | 107(100-115) | 0.156 | 0.163 | 749 |
| IN718-55 m/min | *unworn* | 341(321-361) | 162(149-174) | 0.226 | 0.039 | 621 |
| | $\mu_2$=0.4 | 334(316-351) | 203(192-214) | 0.192 | 0.048 | 608 |
| | $\mu_2$=0.5 | 348(329-368) | 218(207-228) | 0.192 | 0.026 | 621 |
| | $\mu_2$=0.6 | 365(345-386) | 227(216-238) | 0.191 | 0.031 | 633 |
| IN718-90 m/min | *unworn* | 333(305-361) | 167(152-182) | 0.226 | 0.052 | 639 |
| | $\mu_2$=0.4 | 332(312-352) | 205(194-216) | 0.187 | 0.068 | 703 |
| | $\mu_2$=0.5 | 350(330-369) | 213(202-224) | 0.189 | 0.044 | 682 |
| | $\mu_2$=0.6 | 370(353-387) | 232(222-241) | 0.184 | 0.025 | 716 |

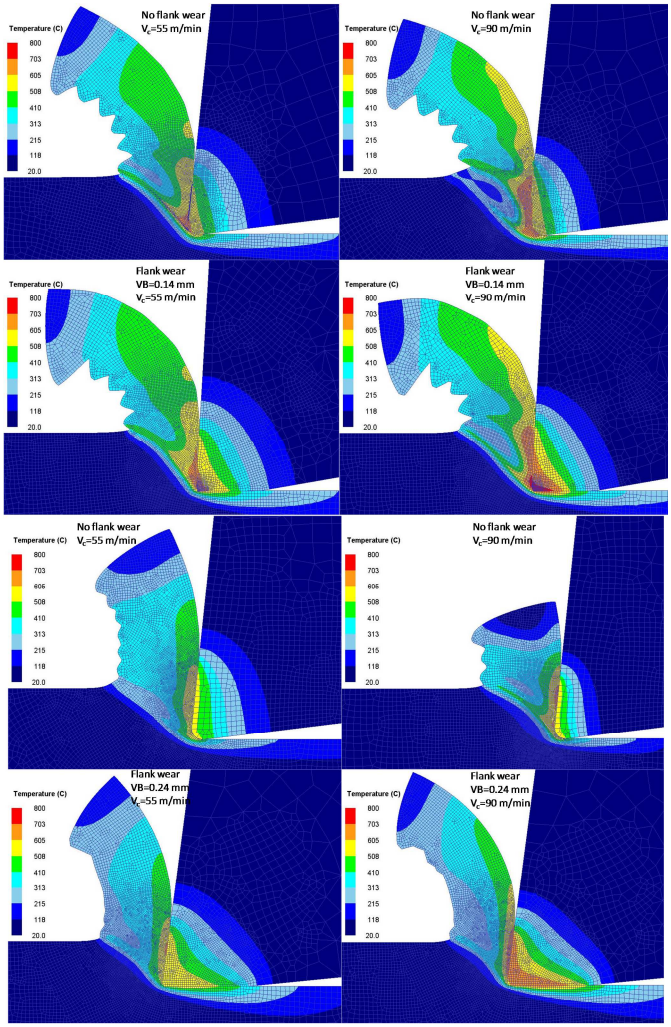


Fig.7: Effect of flank wear on temperatures after turning Ti-Al6-4V (left) and IN718 (right).

**Machining Induced Surface Integrity**

After machining processes, the workpiece material is released of the thermomechanical load, the stresses that remain in the material after the loading is removed are called residual stresses. They are considered to be due to mainly machining induced plastic deformation in the subsurface of the workpiece material and thermal effects at the surface due to tool wear and friction. The residual stresses are more tensile at the surface of the workpiece and become compressive as the depth of the workpiece increases to around 50 µm. Then, after approximately 300 µm, the residual stresses diminish. The layer that exhibits tensile residual stresses can be related to white layer formation and the compressive residual stresses after 50 µm can be related to dark layer formation [1-6]. It is the general observance that an increase in feed rate makes the residual stresses more tensile at the surface and more compressive in the peak compressive depth, especially at higher cutting speeds, where the peak residual stresses might become less compressive with increasing feed in lower cutting speeds [1-6]. In the presence of tool flank wear the residual stress profiles change and become more tensile. The effects of flank wear on residual stress (in axial direction) are investigated by Chen et al. [19] for Ti-6Al-4V (see Fig. 8) and Sharman et al. [20] for IN718 (see Fig. 8). Circumferential stresses (in the direction of cutting velocity vector) are mainly compressive on the machined surface when using a fresh unworn tool. However, circumferential stresses turn tensile when cutting with a worn tool or in presence of tool flank contact. This is consistent with the residual stress predictions for machining both Ti-6Al-4V titanium alloy and IN718 nickel alloy as it is shown in Figs. 9 and 10. In addition, prediction of circumferential stress fields is not influenced by friction coefficient in the flank wear land in FE simulations. Influence of cutting speed on the circumferential stresses can also be considered insignificant.

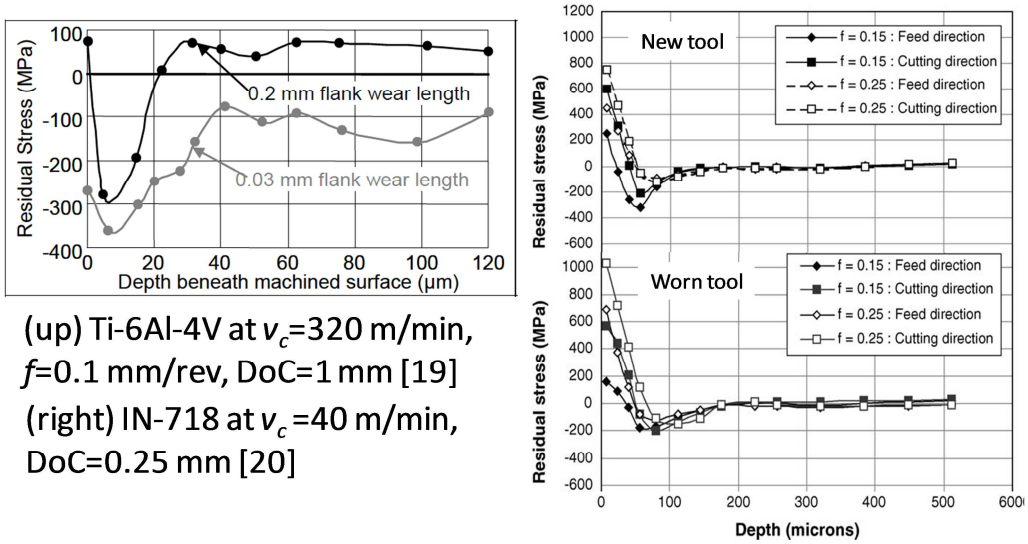


(up) Ti-6Al-4V at $v_c$=320 m/min, $f$=0.1 mm/rev, DoC=1 mm [19]
(right) IN-718 at $v_c$ =40 m/min, DoC=0.25 mm [20]

Fig. 8: Residual stresses measured in after turning of Ti-6AL-4V and IN718.

FE simulation predictions in machining Ti-6Al-4V alloy indicated that axial stresses (in the direction of feed/thrust force) are mainly very small or compressive on the machined surface and turn tensile until about 50 µm depth beneath the surface and become compressive into the depth of machined surface as shown in Fig. 9. Increased cutting speed from 55 to 90 m/min tends to make the residual stresses more compressive and friction coefficient on the flank wear land tends to affect axial stress moderately.

In machining IN718 nickel alloy, unworn tool remains mostly tensile whereas worn tool induces compressive residual stresses. Increasing cutting speed makes axial stress more tensile when using unworn fresh tool as shown in Fig. 10. Effect of tool flank friction coefficient on predicted residual stresses is also apparent. These simulation results show similar patterns with the experimental ones reported in [19] and [20]. Further experimental validations of these predictions are required and left as future work.

## Conclusions

In this study, FE simulations to predict machining induced residual stresses in Ti-6Al-4V titanium and IN718 nickel alloys using modified material constitutive models and elastic-viscoplastic finite element formulation are investigated. Adiabatic shearing based simulation of serrated chips is accomplished. Friction analysis is utilized to determine the friction coefficients on tool rake and flank faces and influence of friction coefficient on predicted residual stress profiles is explored. It is concluded that predicted residual stresses are influenced by the tool flank wear as they become more compressive in machining of IN718 nickel alloy.

## Acknowledgements

The financial support provided by the National Science Foundation (grant number CMMI-0758820), support for DEFORM software by SFTC, Ohio, USA and contributions from CIRP Collaborative Working Group on Surface Integrity are gratefully acknowledged.

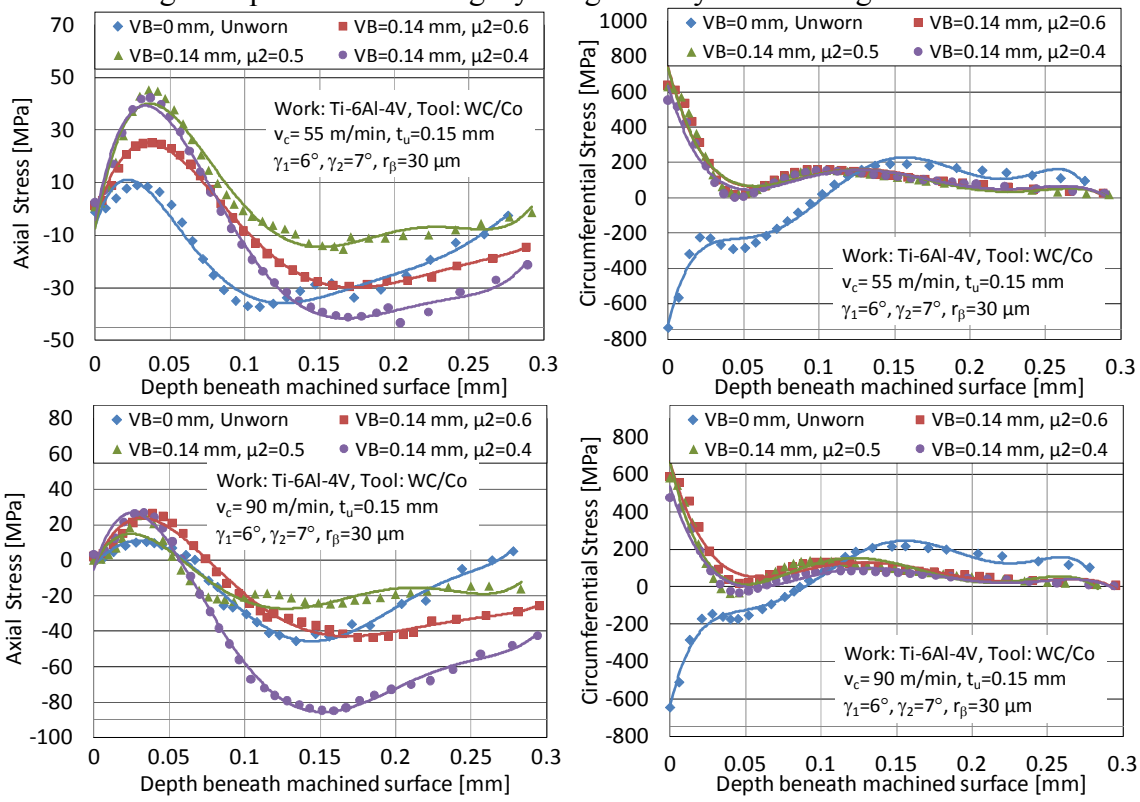


Fig. 9: Effect of friction at flank wear land on residual stresses after turning Ti-Al6-4V.

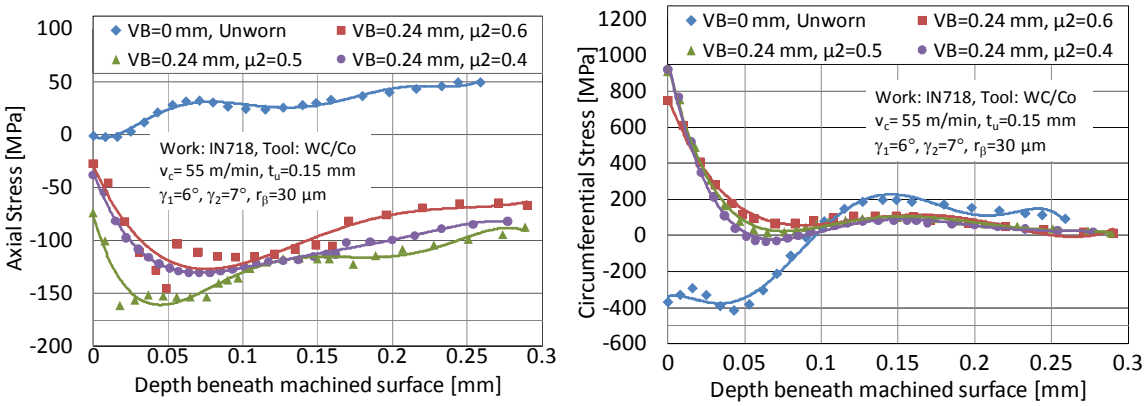

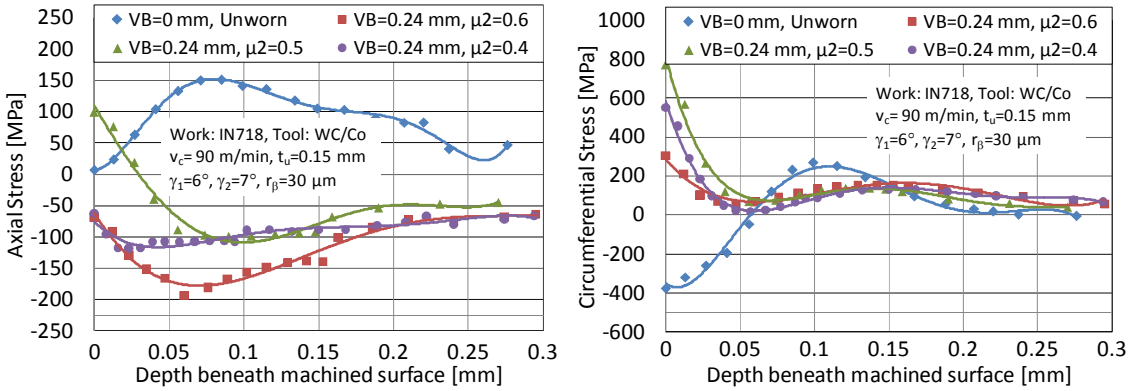


Fig. 10: Effect of friction at flank wear land on residual stresses after turning IN718.

## References


[1] J.C. Outeiro, J.C. Pina, R. M'Saoubi, F. Pusavec and I.S. Jawahir: CIRP Annals – Manuf. Technol. Vol. 57/1 (2008), pp. 77-80.

[2] C.H. Che-Haron and A. Jawaid: J. Mater. Proc. Technol. Vol. 166 (2005), pp. 188-192.

[3] R.S. Pawade, S.S. Joshi and P.K. Brahmankar: Int. J. Mach. Tool Manu. Vol. 48 (2008), pp.15-28.

[4] R. M'Saoubi, J.C. Outeiro, H. Chandrasekaran, O.W. Dillon Jr. and I.S. Jawahir, Int. J. Sus. Manuf. Vol. 1/1-2. (2008), pp. 203-236.

[5] Y.B. Guo, W. Li and I.S. Jawahir: Mach. Sci. Technol. Vol. 13 (2009), pp. 437-470.

[6] D. Ulutan and T.Özel: Int. J. Mach. Tool Manu. Vol. 51 (2009), pp. 2250-280.

[7] M. Calamaz, D. Coupard and F. Girot: Int. J. Mach. Tool Manu. Vol. 48 (2008), pp. 275–288.

[8] M. Sima and T. Özel: Int. J. Mach. Tool Manu. (2010) Vol. 50, pp. 943–960.

[9] W.-S. Lee and C.-F. Lin: Mater. Sci. Eng. A241 (1998), pp. 48-59.

[10] J.M. Zhang, Z.Y. Gao, J.Y. Zhuang, Z.Y. Zhong and P. Janschek: J. Mater. Proc. Technol. Vol. 70 (1997), pp. 252-257.

[11] J.J. DeMange, J.M. Pereira, B.A. Lerch and V. Prakash, in: *Proceedings of the SEM IX International Congress on Experimental Mechanics*, Orlando, FL, (2000) June 5-8, pp. 344-347.

[12] J.M. Pereira and B.A. Lerch: Int. J. Impact Eng. Vol. 25 (2001), pp. 715-733.

[13] E. Uhlmann, M. Graf von der Schulenburg and R. Zettier: CIRP Annals – Manuf. Technol. Vol. 56/1 (2007), pp. 61-64.

[14] R. Sievert, H.D. Noack, A. Hamann, P. Loewe, K.N. Singh, G. Kuenecke, R. Clos, U. Schreppel, P. Veit, E. Uhlmann and R. Zettier: Techniche Mechanik, Vol. 23/2-4 (2003), pp. 216-233.

[15] J. Olschewski, A. Hamann and M. Bendig: *Werkstoffmechanik einer Nickelbasislegierung beim Hochgeschwindigkeitsspanen- Werkstoffverhalten und Modellierung*, Teil II, Report BAM-V.2 01/3 (2001), Bundesanstalt für Materialforschung und prüfung (BAM), Berlin.

[16] J. Lorentzon, N. Järvstråt and B.L. Josefson: J. Mater. Proc. Technol. Vol. 209 (2009), pp. 4645-4653.

[17] A.V. Mitrofanov, V.I. Babitsky and V.V. Silberschmidt: Comput. Mater. Sci. Vol. 32/3-4 (2005), pp. 463-471.

[18] C-F.Wyen and K. Wegener: CIRP Annals – Manuf. Technol. Vol. 59/1 (2010), pp. 93-96.

[19] L. Chen, T.I. El-Wardany and W.C. Harris: CIRP Annals – Manuf. Technol. Vol. 53/1 (2004), pp. 95-98.

[20] A.R.C. Sharman, J.I. Hughes and K. Ridgway: J. Mater. Proc. Technol. Vol.173 (2006), pp. 359-367.

**Modelling of Machining Operations**
doi:10.4028/www.scientific.net/AMR.223

**Prediction of Machining Induced Surface Integrity Using Elastic-Viscoplastic Simulations and Temperature-Dependent Flow Softening Material Models in Titanium and Nickel-Based Alloys**
doi:10.4028/www.scientific.net/AMR.223.401